The Astrophysical Journal, 960:22 (12pp), 2024 January 1 https://doi.org/10.3847/1538-4357/ad0547

Formation of Interstellar Complex Organic Molecules on Water-rich Ices Triggered by Atomic Carbon Freezing

Stefano Ferrero[1], Cecilia Ceccarelli[2], Piero Ugliengo[3], Mariona Sodupe[1], and Albert Rimola[1]
[1] Departament de Química, Universitat Autònoma de Barcelona, Bellaterra, E-08193, Catalonia, Spain; mariona.sodupe@uab.cat, albert.rimola@uab.cat
[2] Univ. Grenoble Alpes, CNRS, Institut de Planétologie et d'Astrophysique de Grenoble (IPAG), F-38000 Grenoble, France
[3] Dipartimento di Chimica and Nanostructured Interfaces and Surfaces (NIS) Centre, Università degli Studi di Torino, via P. Giuria 7, I-10125, Torino, Italy
Received 2023 July 18; revised 2023 October 4; accepted 2023 October 18; published 2023 December 19

Abstract

The reactivity of interstellar carbon atoms (C) on water-dominated ices is one of the possible ways to form interstellar complex organic molecules (iCOMs). In this work, we report a quantum chemical study of the coupling reaction of C (^{3}P) with an icy water molecule, alongside possible subsequent reactions with the most abundant closed-shell frozen species (NH_3, CO, CO_2, and H_2), atoms (H, N, and O), and molecular radicals (OH, NH_2, and CH_3). We found that C reacts spontaneously with the water molecule, resulting in the formation of ^{3}C–OH_2, a highly reactive species due to its triplet electronic state. While reactions with the closed-shell species do not show any reactivity, reactions with N and O form CN and CO, respectively, the latter ending up in methanol upon subsequent hydrogenation. The reactions with OH, CH_3, and NH_2 form methanediol, ethanol, and methanimine, respectively, upon subsequent hydrogenation. We also propose an explanation for methane formation observed in experiments through additions of H to C in the presence of ices. The astrochemical implications of this work are: (i) atomic C on water ice is locked into ^{3}C–OH_2, making difficult the reactivity of bare C atoms on icy surfaces, contrary to what is assumed in current astrochemical models; and (ii) the extraordinary reactivity of ^{3}C–OH_2 provides new routes toward the formation of iCOMs in a nonenergetic way, in particular ethanol, the mother of other iCOMs once it is in the gas phase.

Unified Astronomy Thesaurus concepts: Astrochemistry (75); Interstellar medium (847); Interstellar molecules (849); Interstellar dust (836); Surface ices (2117); Complex organic molecules (2256); Reaction rates (2081); Computational methods (1965)

1. Introduction

Improving our understanding of the formation of molecules at the cryogenic temperatures of interstellar molecular clouds is of paramount importance to fully understand their chemical evolution (diversity and complexity). The surfaces of interstellar grains—submicrometer-sized particles present in the molecular clouds and well mixed with the gas—are potential sites where reactions forming interstellar molecules can take place (e.g., Allen & Robinson 1975; Duley et al. 1978; Tielens & Hagen 1982). This is because grains can play different roles in these synthesis reactions: (i) as chemical catalysts, by reducing the activation energies (Watanabe & Kouchi 2008; Cuppen et al. 2017; Zamirri et al. 2019); (ii) as third bodies, through which the reaction energies can be dissipated, hence stabilizing the newly formed species (Cuppen et al. 2017; Zamirri et al. 2019); (iii) as reactant concentrators, which retain the reactive species and allow their diffusion on the surfaces for an eventual reactive encounter (Hama & Watanabe 2013; Cuppen et al. 2017; Zamirri et al. 2019; Ceccarelli et al. 2023); and (iv) in the case of ices, as reactant suppliers, since icy components can be converted into reactive derivatives ready to react (e.g., generation of radicals upon UV incidence) (Öberg 2016; Ceccarelli et al. 2023).

In general, interstellar grains are made of a refractory core, consisting of silicate or carbonaceous materials (e.g., Henning 2010; Jones et al. 2013, 2017), and, in the coldest and densest regions of the interstellar medium (ISM), are coated with icy mantles (e.g., Boogert et al. 2015). The grain mantles are principally made of water and other molecules (e.g., CO, CO_2, NH_3, CH_3OH, CH_4, among others) in smaller quantities, detected by employing infrared (IR) spectroscopic observations (e.g., Boogert et al. 2015; Yang et al. 2022; McClure et al. 2023). An important constraint on the possible interstellar chemical reactions is set by the very low temperatures ($\leqslant$10 K in molecular clouds), which only permit essentially barrierless reactions or reactions with a very low energy barrier to be efficient, unless external energetic inputs are involved (e.g., Schutte et al. 1992; Bernstein et al. 1995, 1999; Strazzulla 1997; Palumbo et al. 1999) and/or quantum tunneling effects dominate (e.g., Andersson et al. 2011; Meisner & Kästner 2016; Meisner et al. 2017; Miksch et al. 2021; Molpeceres & Kästner 2021; Molpeceres & Rivilla 2022; Molpeceres et al. 2022, 2023a).

Among the different astrochemically relevant compounds, those called interstellar complex organic molecules (iCOMs) enjoy a particularly important position (Herbst & van Dishoeck 2009; Ceccarelli et al. 2017). iCOMs are molecules with 6–13 atoms in which at least one is C, alongside other heteroatoms (O, N, S...), constituting organic compounds. Examples of often detected iCOMs are acetaldehyde (CH_3CHO), formamide (NH_2CHO), methyl formate (CH_3OCHO) and dimethyl ether (CH_3OCH_3) (e.g., see the latest reviews by Jørgensen et al. 2020; Ceccarelli et al. 2023). Although they are very small and simple molecules when compared to terrestrial ones, iCOMs have gained great attention in the last two decades because some of them are actual biomolecule precursors, the possible molecular building blocks of biological systems, and are detected in star-forming regions that will

eventually give rise to solar-like planetary systems (Cazaux et al. 2003). Therefore, iCOMs may represent primogenial organic chemistry and could have played a role in the emergence of life on Earth.

The first detections of iCOMs were obtained toward massive star-forming regions, in so-called hot cores (e.g., Rubin et al. 1971; Blake et al. 1987), and only almost 30 yr later in solar-like protostar hot corinos (Ceccarelli et al. 2000; Cazaux et al. 2003). More recently, iCOMs have been detected in cold prestellar cores (e.g., Bacmann et al. 2012; Cernicharo et al. 2012; Vastel et al. 2014; Scibelli & Shirley 2020), protostellar outflows (e.g., Arce et al. 2008; Codella et al. 2009, 2017; Lefloch et al. 2017; De Simone et al. 2020), protoplanetary disks (Öberg et al. 2015; Walsh et al. 2016; Favre et al. 2018; Ilee et al. 2021), and even external galaxies (e.g., Henkel et al. 1987; Muller et al. 2011; Martín et al. 2021). At present, more than 290 molecular species have been detected in different astrophysical environments, among which approximately 25 are iCOMs (McGuire 2022).[4]

The formation of iCOMs has been postulated to occur in the gas phase and/or on the icy surfaces of grains. In the latter, a prevailing mechanism advocates the coupling between two radical species that were previously formed in situ by UV incidence on the ice mantles (e.g., Garrod 2013; Iqbal & Wakelam 2018; Suzuki et al. 2018). However, it has recently been shown that radical–radical reactions on water ices may exhibit activation barriers depending on the ice composition, surface morphology, type of adsorption site, binding energy of the reactive radicals with the surface, and the relative orientation of the reactive radicals (e.g., Enrique-Romero et al. 2022). Furthermore, reactive radicals need to encounter each other via surface diffusion, which is affected by all these factors, and is not trivial due to the very low interstellar temperatures (e.g., Enrique-Romero et al. 2021).

Because of that, alternative grain-surface reaction mechanisms for iCOM formation have been proposed such as the radical–ice one, in which a radical reacts directly with a component of the ice through an Eley–Rideal mechanism (Rimola et al. 2018; Perrero et al. 2022; Ferrero et al. 2023a). In this context, a promising route toward iCOM formation is based on the high reactivity of atomic C. On the surfaces of grains, the carbon atom, either in its ground electronic state (C, ^{3}P) or in its cationic form (C^+, ^{2}P), is indeed a highly reactive species and reacts barrierlessly with several components. Hence, the reaction of C atoms with molecules of the ice mantles could give rise to a variety of interstellar molecules, including iCOMs (Krasnokutski et al. 2017, 2020, 2022; Henning & Krasnokutski 2019; Qasim et al. 2020; Molpeceres et al. 2021; Potapov et al. 2021; Woon 2021; Fedoseev et al. 2022; Ferrero et al. 2023a).

The formation of methane from the hydrogenation of carbon atoms is one of the first reactions evoked to occur on the icy surfaces of interstellar grains (e.g., Tielens & Hagen 1982; Cuppen et al. 2017). Only recently, the formation of CH_4 on water ice by hydrogenation of C was observed experimentally when co-depositing atomic C and H with H_2O at cryogenic temperatures (Qasim et al. 2020). Similarly, the formation of CH_4 was also demonstrated experimentally by the reaction of C with H_2 on water ice (Lamberts et al. 2022). Moreover, in a combined theoretical and experimental work, it was shown that C (^{3}P) adsorbed on water ice mantles reacts with the oxygen atom of an icy water molecule to form a C–OH_2 species, stable in the electronic triplet excited state, which, upon a water-assisted proton transfer followed by an intersystem crossing (ISC) toward the fundamental singlet state, evolves into formaldehyde (H_2CO) (Molpeceres et al. 2021). Finally, a very recent experimental paper provided evidence of possible diffusion of carbon atoms on the surface of interstellar ice (Tsuge et al. 2023). These works thus show how complicated carbon chemistry on interstellar ice is, and that different outcomes, depending on a variety of factors, are possible upon adsorption.

The above-mentioned theoretical studies show the great importance of performing accurate quantum-mechanical (QM) computations to correctly understand the experimental results (which will be done here in Section 4). An analysis of the electronic structure of the ^{3}C–OH_2 species indicates that the unpaired electrons (responsible for the triplet electronic state) remain mostly localized on the C end. Thus, the enhanced reactivity of the initial C (^{3}P) atom is transferred to the newly formed ^{3}C–OH_2 species. This is of relevance because it opens the possibility that ^{3}C–OH_2 is an activated species that can trigger the formation of interstellar molecules through non-energetic pathways, likely presenting very small or no barriers.

In this work, we present results based on QM simulations to verify this hypothesis. This has been done by studying, first, the adsorption of atomic C on the surfaces of interstellar water ice grains, in which the ^{3}C–OH_2 species forms, followed by its reactivity with relatively abundant interstellar species of a different nature, that is: (i) closed-shell species, abundant on the water-dominated ices (NH_3, CO, CO_2, and H_2); (ii) atoms that can be found as adsorbed species on the ice surfaces (H, N, and O); and (iii) molecular radicals also trapped on the ices (CH_3, NH_2, and OH), which could be the product of the partial hydrogenation of atoms/molecules (e.g., Taquet et al. 2012) or the in situ formation by energetic irradiation (UV photons or cosmic-ray particles) (e.g., Garrod 2013).

The article is organized as follows. Section 2 describes the adopted methodology, Section 3 shows the obtained results, Section 4 discusses the consequences of these results, and Section 5 concludes the article.

2. Computational Details

All the simulations are grounded on the density functional theory (DFT) and have been performed using the Orca software (Neese et al. 2020). The range-separated DFT hybrid ωB97X-V method has been used due to its overall good performance among other hybrid functionals (Goerigk et al. 2017). Dispersion interactions are taken into account by employing the VV10 nonlocal correlation (Vydrov & Van Voorhis 2010). Ahlrich's def2-TZVP has been used as the basis set for all the calculations (Weigend & Ahlrichs 2005). It is worth mentioning that similar functionals (i.e., ωB97X-D3 and ωB97X-D4, differing only in the definition for the description of dispersion interactions) have been shown to provide results in good agreement with the highly correlated CCSD(T) results (giving errors in energy barriers less than 10%), and hence are accurate enough to describe reactions with energy barriers similar to those presented in this work (Perrero et al. 2022; Ferrero et al. 2023a). Geometric optimizations have been carried out employing the geometrical counterpoise correction (Kruse & Grimme 2012) to palliate the superposition error in the basis set

[4] https://cdms.astro.uni-koeln.de/classic/molecules

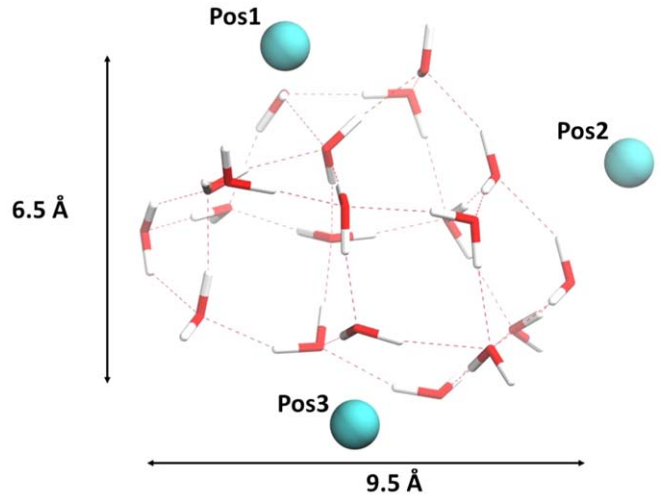

Figure 1. The $(H_2O)_{20}$ cluster model used in this work, optimized at ωB97X-V/def2-TZVP, showing its dimensions. The different positions at which the C atom has been adsorbed (Pos1, Pos2, and Pos3) are also shown.

(Liu & McLean 1973). Open-shell systems have been treated with the unrestricted formalism. Electron spin densities and net charges on the atoms have been obtained through a Löwdin population analysis.

The interstellar ice has been modeled by adopting a cluster approach. It consists of a cluster model of 20 water molecules taken from Shimonishi et al. (2018) and optimized at our level of theory. The cluster has an ellipsoid-like shape, with axes of approximately 6.5 and 9.5 Å (see Figure 1). Considering that the adsorption of atomic C and the subsequent reactivity are local surface phenomena (i.e., occurring on single binding and reaction sites), this cluster has been chosen as a good trade-off between the representativity of an actual interstellar amorphous water ice surface and the computational cost of the calculations.

Harmonic vibrational frequencies have been calculated to (i) characterize the nature of the stationary points of the calculated potential energy surfaces (PESs), i.e., reactants, products, and intermediates as minima of the PESs, and transition states as first-order saddle points of the PESs, and (ii) take into account the vibrational zero-point energy (ZPE) of each stationary point to obtain ZPE-corrected energetics. The ZPE-corrected interaction energy of atomic C on the water ice model was calculated as

$$\Delta H(0) = E_{\rm complex} - E_{\rm ice} - E_{\rm C} \quad (1)$$

where $E_{\rm complex}$ and $E_{\rm ice}$ are the ZPE-corrected absolute potential energies for the carbon adsorbed on the water ice cluster and for the isolated optimized water ice cluster, and $E_{\rm C}$ is the absolute potential energy for the isolated carbon atom. Transition state structures have been localized adopting the climbing-image nudged elastic band (CI-NEB) technique implemented in Orca (Ásgeirsson et al. 2021). ZPE-corrected energy barriers of the explored reactions have been calculated as

$$\Delta H^{\ddagger}(0) = E_{\rm TS} - E_{\rm min} \quad (2)$$

where $E_{\rm TS}$ and $E_{\rm min}$ are the ZPE-corrected absolute potential energies for the transition state (TS) and the minimum structure of the reaction, respectively. Note that at 0 K, the absolute ZPE-corrected energy is equal to the absolute enthalpy, i.e., $E = H(0)$, hence our notation in terms of enthalpy variation at 0 K for the interaction energies and energy barriers. The visual molecular dynamics software was used for the display and manipulation of the structures and for image creation (Humphrey et al. 1996).

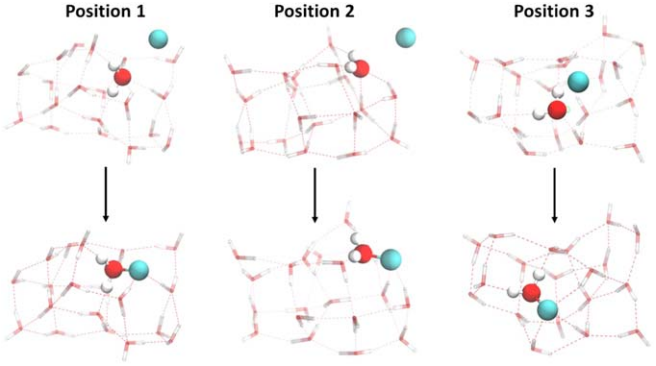

Figure 2. ωB97X-V-optimized structures for C atom on the $(H_2O)_{20}$ cluster model, which results in the formation of a C–OH_2 species. The initial guessed structures of the three different positions (Pos1, Pos2, and Pos3) are also shown. The reactive species are represented as ball and sticks, while the rest of the water molecules of the cluster are shown as tubes. The color code for the atoms is H in white, C in pale green, and O in red.

3. Results

3.1. Carbon Condensation on Water Ice

To simulate the adsorption of atomic C (^{3}P) on water ice, the two partners (i.e., the C atom and the $(H_2O)_{20}$ cluster) were placed 3.0 Å apart from each other and their geometries were then optimized. Three initial structures, differing in the position of the C atom around the cluster, have been guessed (see Figure 1). The selection of the positions was based on considerations of surface morphology and coordination (according to the Fowler rules) of the H_2O molecule that reacts with atomic C. That is: C reacts in Pos1 with an O-undercoordinated water molecule belonging to a small cavity in the surface, in Pos2 with a completely coordinated water molecule, and in Pos3 with an O-undercoordinated water molecule belonging to a flat part of the surface. As a result, for each initial position, the spontaneous reaction between the C atom and a water molecule of the ice takes place during the geometric optimizations, forming the C–OH_2 species (depicted in Figure 2), which due to the spin conservation rule is in the triplet electronic state.

The formation of this ^{3}C–OH_2 species was already observed in the computational studies of Hwang et al. (1999), Shimonishi et al. (2018), Molpeceres et al. (2021), and Lamberts et al. (2022). For the three initial positions considered in this work, the calculated interaction energies ($\Delta H(0)$) of the C atom with the water cluster are reported in Table 1, alongside the C–O bond lengths and the charges and spin densities on the C and O atoms of the C–OH_2 species.

Both the calculated $\Delta H(0)$ and the C–O distances are in very good agreement with those reported by Shimonishi et al. (2018) and Molpeceres et al. (2021). The values reported by Lamberts et al. (2022) are lower than the ones computed here. This is because the systems adopted by those authors refer to the coupling of the C atom with one isolated molecule (-52.9 kJ mol^{-1}) and with the $(H_2O)_3$ water trimer cluster (-95.2 kJ mol^{-1}). Interestingly, by increasing the cluster size,

Table 1
Computed ZPE-corrected Interaction Energies $\Delta H(0)$ of the C Atom with the Water Ice Surface Cluster Model, Considering the Three Positions

Position	$\Delta H(0)$ (kJ mol^{-1})	C–O Length (Å)	Charges	Spin Densities		
				O	C	O
Pos1	−116.2	1.49	−0.52	0.06	1.77	0.08
Pos2	−115.0	1.49	−0.53	0.09	1.73	0.10
Pos3	−110.2	1.50	−0.55	0.08	1.72	0.09

Note. The C–O bond lengths, the Löwdin net atomic charges, and the electronic spin densities of the C and O atoms of the optimized ^{3}C–OH$_2$ species on the water cluster are also listed.

the reaction energy of the coupling between C and a water molecule increases considerably, tending to our obtained values. Because the coupling reaction of C (^{3}P) with a water molecule of the ice gives rise to the ^{3}C–OH$_2$, this adsorption event can be classified as chemisorption. According to the electronic spin densities, the C atom retains its two unpaired electrons upon the formation of ^{3}C–OH$_2$ and, accordingly, this species is expected to be reactive through its C atom. Thus, the ^{3}C–OH$_2$ species can be understood as a carbon reactive center, that is, like an activated complex that reacts through its C atom with other species that can diffuse in its proximity or land from the gas phase on surface sites close to it. Moreover, according to the Löwdin atomic charges, the carbon atom presents a negative net charge, which renders this atom a good H-bond acceptor, like the oxygen in water. These two facts will have important consequences for the chemical properties of the carbon reactive center, as we will see in the following.

3.2. Reactivity of the Carbon Reactive Center with Abundant Closed-shell Molecules: NH_3, CO, CO_2, and H_2

The reactivity with the relatively abundant molecular constituents of interstellar icy mantles (NH_3, CO, CO_2) and the most abundant molecule of the ISM (H_2) has been studied by placing them 2.5 Å away from the C atom of the ^{3}C–OH$_2$ species, considering the three different positions as depicted in Figure 2. With any of the molecules tested, no spontaneous reaction is observed during the geometric optimization (performed at a total triplet electronic state), resulting in the systems represented in Figure 3. Results indicate that the molecular species prefer to interact through hydrogen bonds (for the CO, CO_2, and NH_3 cases) or dispersion interactions (for the H_2 case) with either the water molecules of the ice or the C atom of ^{3}C–OH$_2$ (for the NH_3 case) due to its negative atomic charge (see above); in this latter situation C acts similarly to a dangling oxygen of water ice.

3.3. Reactivity of the Carbon Reactive Center with Abundant Atoms: H, N, and O

Based on the interstellar abundances and the mobility of atoms on the ice mantles, the highest probability that the ^{3}C–OH$_2$ has a reactive encounter is with atomic hydrogen, followed by atomic nitrogen and oxygen. Therefore, the reactions between the carbon reactive center and these three atomic species have been studied.

H. To simulate the reaction with H, an H atom was placed 2.5 Å away from the ^{3}C–OH$_2$ derived from Pos1, Pos2, and Pos3, and the geometries of these initial guessed structures were optimized in a doublet spin state, because this is the reactive multiplicity (in contrast to the unreactive quartet state). In this process, the H atom spontaneously makes a chemical bond with the carbon atom of ^{3}C–OH$_2$, forming the ^{2}HC–OH$_2$ radical species, which remains adsorbed on the ice cluster. This species, in a similar way to the ^{3}C–OH$_2$ one, can also be regarded as a carbon reactive center due to its doublet radical character, which is still mainly localized on the carbon end. Therefore, a second H atom was also added. As before, this second H atom spontaneously forms a chemical bond with the carbon reactive center, creating a closed-shell H$_2$C–OH$_2$ species. Interestingly, the optimization process of the second addition of H for the system arising from Pos1 is associated with a spontaneous water-assisted proton transfer, in which one proton linked to the water end of the H$_2$C–OH$_2$ species is transferred to the C atom through water molecules of the ice model, finally forming methanol (CH_3OH) in a barrierless way. That is, H$_2$C–OHH* → CH$_2$H*–OH, in which H* is the transferred atom. Figure 4(A) shows a snapshot of the geometric optimization, in which the water-assisted proton transfer process is highlighted.

In view of the possibility of this conversion to form methanol, we run NEB calculations for the other two cases (Pos2 and Pos3) to characterize the minimum energy path and calculate the energy barrier for the formation of methanol adopting a similar mechanism. The obtained results (shown in Figures 4(B) and (C)) indicate that, in both cases, the process presents a very small potential barrier ($\leqslant$4 kJ mol^{-1}), which moreover becomes submerged when the ZPE corrections are introduced.

Thus, in practice, the two surface reactions studied here are (the multiplicity of each species is indicated by the left superscript)

$$^2\mathrm{H} + {}^3\mathrm{C–OH_2} \longrightarrow {}^2\mathrm{HC–OH_2} \quad (3)$$

$$^2\mathrm{H} + {}^2\mathrm{HC–OH_2} \longrightarrow \mathrm{CH_3OH}. \quad (4)$$

These results indicate therefore that even at the cryogenic temperatures of the cold molecular clouds, the formation of CH_3OH through this chemical route is efficient due to the high reactivity of the carbon reactive center alongside the abundance and high mobility of the hydrogen atom on the interstellar ice surfaces.

N and O. Now, let us focus on the reactions with atomic N and O, which have been studied in the same way as H. The fundamental electronic state of atomic nitrogen is ^{4}S and that of oxygen ^{3}P. Thus, the total reactive electronic spin multiplicities with ^{3}C–OH$_2$ are doublet and singlet, respectively. During the optimization process, the atoms approach the C–OH$_2$ and, in a spontaneous and concerted way, they establish a chemical bond with the carbon atom, forming the radical CN$^\cdot$ and the neutral CO species, in both cases breaking the original C–O bond of the carbon reactive center (see Figure 5) and releasing H_2O. In summary, the two surface reactions studied here are

$$\mathrm{N}(^4\mathrm{S}) + {}^3\mathrm{C–OH_2} \longrightarrow {}^2\mathrm{CN}^\cdot + \mathrm{H_2O} \quad (5)$$

$$\mathrm{O}(^3\mathrm{P}) + {}^3\mathrm{C–OH_2} \longrightarrow {}^1\mathrm{CO} + \mathrm{H_2O}. \quad (6)$$

The reason why in these cases the OH$_2$ moiety of the carbon reactive center detaches from the C atom is of thermodynamic nature: there is a large energy gain by forming the triple C≡O and C≡N chemical bonds (reaction energies of −684 and −958 kJ mol^{-1}, respectively), in detriment to breaking the single C–O bond. Such reaction energies are expected to be efficiently absorbed and dissipated throughout the ice (as

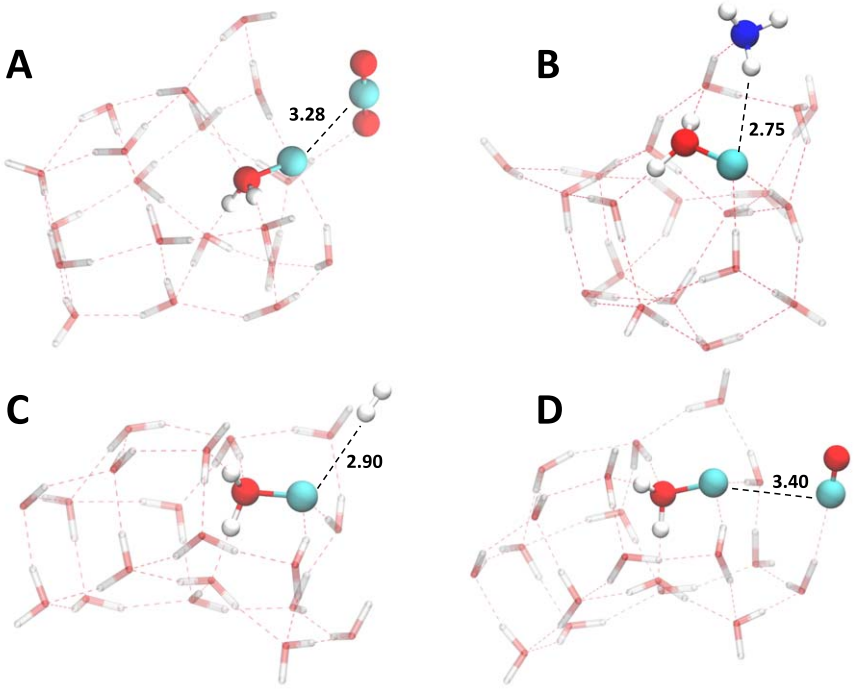

Figure 3. Optimized geometry of the closed-shell species on the water cluster with the carbon reactive center. (A) CO_2 optimized geometry in Pos1. (B) NH_3 optimized geometry in Pos2. (C) H_2 optimized geometry in Pos3. (D) CO optimized geometry in Pos1. In all the panels the adsorbed molecules plus the C–OH_2 species are highlighted in the ball and stick representation. Distances (in Å) between the carbon atom of the C–OH_2 moiety and the closest atom of the adsorbed species are highlighted with a black dashed line. The color code for the atoms is H in white, C in pale green, N in blue, and O in red.

shown in computational works regarding energy dissipation of large exothermic reactions (e.g., Pantaleone et al. 2020, 2021; Molpeceres et al. 2023b) due to vibrational coupling (Ferrero et al. 2023b). However, the amount of energy released by the reactions is very large, and accordingly, side phenomena cannot be discarded. For the case of CO, chemical desorption (namely, the desorption of a chemical species upon its formation owing to the local heating caused by the exothermicity of the reaction) could occur, since the binding energy of CO on water is relatively low (Ferrero et al. 2020). For the case of $CN^{\cdot}$, the reaction energy could be used to proceed with subsequent chemical reactions. Indeed, Rimola et al. (2018) postulated the reactivity of radical $CN^{\cdot}$ with icy water molecules, first forming NH_2CO and then, following an addition of H, finally forming NH_2CHO. This reaction could well take place once $CN^{\cdot}$ forms by the reaction of N with C–OH_2.

3.4. Reactivity of the Carbon Reactive Center with Abundant Radicals: OH, CH_3, and NH_2

The reactions of these three radical species have been studied adopting the same approach as that used for the atomic species, that is, by placing the radicals 2.5 Å away from the ^{3}C–OH_2 and optimizing the system in the total reactive electronic state, in this case, the doublet one.

OH and CH_3. For the addition of OH and CH_3 to ^{3}C–OH_2, we found the spontaneous formation of a new chemical bond between the carbon atom of ^{3}C–OH_2 and the O and C atoms of OH and CH_3, respectively, during the geometric optimization, in which the ^{2}HO–C–OH_2 and $^2H_3$C–C–OH_2 species are formed. We observed this behavior in all cases regardless of the initial geometry.

The barrierless reaction paths observed are associated with the following chemical reactions:

$$^2OH + {}^3C\text{–}OH_2 \longrightarrow {}^2HO\text{–}C\text{–}OH_2 \quad (7)$$

$$^2CH_3 + {}^3C\text{–}OH_2 \longrightarrow {}^2H_3C\text{–}C\text{–}OH_2. \quad (8)$$

These reactions are very similar to the first addition of H to the carbon reactive center, and thus the unpaired electron in ^{2}HO–C–OH_2 and $^2H_3$C–C–OH_2 is mostly localized on the carbon atom of the C–OH_2 moiety. Because of this similarity, a second reaction of the ^{2}HO–C–OH_2 and $^2H_3$C–C–OH_2 with an H atom has been investigated to check additional chemical reactivity, and these in turn can evolve to other more stable species through a nonenergetic proton shuttle mechanism.

For the addition of H to ^{2}HO–C–OH_2, two different products have been found. From Pos1 and Pos2, methanediol (OH–CH_2–OH) compound is formed by a barrierless water-assisted proton transfer (see Figure 6(A)). From the remaining position (Pos3), the hydroxycarbene (HOCH) species is formed after the cleavage of the original C–O bond belonging to the ^{3}C–OH_2 species (see Figure 6(B)). Both processes were observed during the geometric optimization and thus they can be considered spontaneous. The observed chemical reactions are

$$^2HO\text{–}C\text{–}OH_2 + {}^2H \longrightarrow {}^1HO\text{–}CH_2\text{–}OH \quad (9)$$

$$^2HO\text{–}C\text{–}OH_2 + {}^2H \longrightarrow {}^1HCOH + H_2O. \quad (10)$$

Interestingly, HCOH as formed in Figure 6(B) was highlighted in the work of Molpeceres et al. (2021) to be a precursor species of formaldehyde (i.e., HCOH → H_2CO). For this reaction, they found a variety of energy barriers ranging (including ZPE correction) from submerged barriers up to 12 kJ mol^{-1}, depending on the binding site of the C atom. In this work, to obtain the activation energy of the HCOH → H_2CO conversion, an NEB calculation

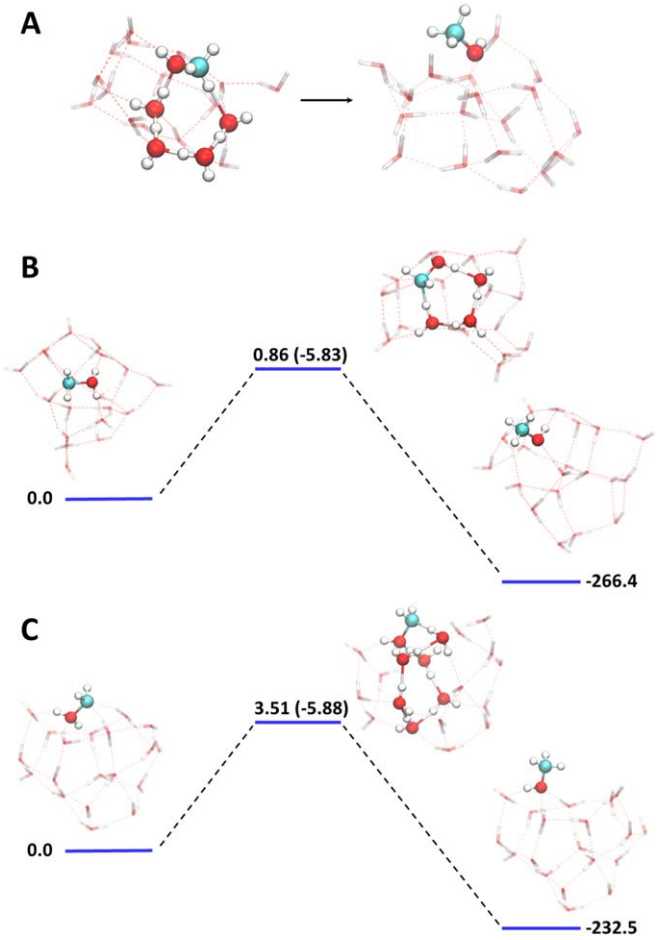

Figure 4. (A) Snapshot of the geometry optimization representing the water-assisted proton transfer mechanism for the $H_2C–OH_2 \rightarrow CH_3–OH$ reaction and of the final product of Pos1. (B), (C) Potential energy surfaces (in kJ mol^{-1}) for the water-assisted proton transfer of Pos2 and Pos3. At the TS structure, the $\Delta H(0)$ is displayed in parenthesis, indicating barrierless reactions. In every panel, the $H_2C–OH_2$ species, the water molecules involved in the proton transfer, and methanol are highlighted in the ball and stick representation. The color code for the atoms is H in white, C in pale green, and O in red.

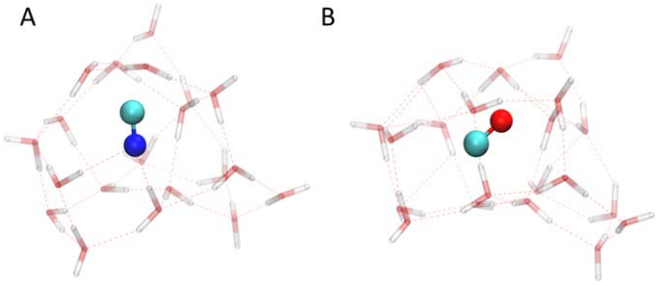

Figure 5. Final products of the reaction of (A) atomic N and (B) atomic O with the $^3C–OH_2$ carbon reactive center on water ice surfaces, which result in the formation of CN^- and CO, respectively. These final species are highlighted in the ball and stick representation. The color code for the atoms is H in white, C in pale green, N in blue, and O in red.

was performed, obtaining a ZPE-corrected energy barrier of 7.9 kJ mol^{-1} (see Figure 7), which lies within the range of values found in Molpeceres et al. (2021). Therefore, this water-assisted proton transfer is not barrierless, in contrast to what we found in the other cases. Nevertheless, it is important to notice that the estimated barrier is a classical potential barrier and that nuclear quantum effects (not accounted for in this work) can significantly affect the kinetics of this process.

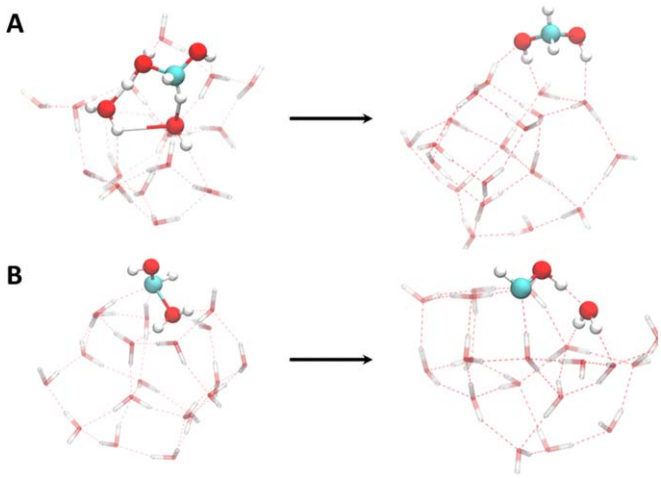

Figure 6. Snapshots of the reactions of the OH radical with the $^3C–OH_2$ carbon reactive center on water ice surfaces. (A) The geometric optimization representing the water-assisted proton transfer mechanism for the $HO–H_2C–OH_2 \rightarrow HO–CH_2–OH$ reaction and the final product are represented. The $HO–H_2C–OH_2$ species and the water molecules involved in the proton transfer are highlighted in the ball and stick representation (left structure) as well as methanediol in the optimized position (right structure). (B) Snapshots of the $HO–HC–OH_2$ intermediate (left structure) during the breaking of the C–O bond and of the HCOH product (right structure) in its optimized geometry. The two species are highlighted in the ball and stick representation. The color code for the atoms is H in white, C in pale green, and O in red.

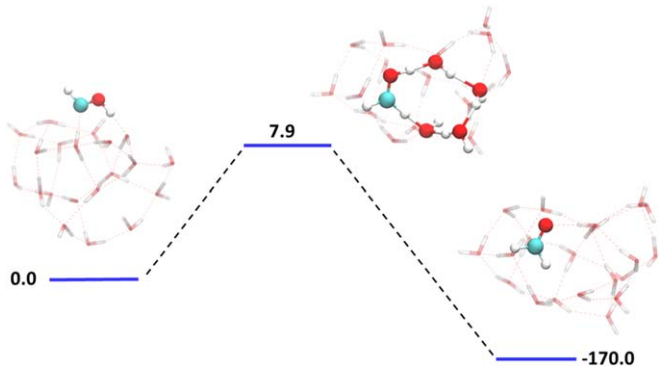

Figure 7. Energy diagram (i.e., reactant, TS, and product) representing the water-assisted proton transfer mechanism for the $HCOH \rightarrow H_2CO$ reaction. ZPE-corrected energies are reported in kJ mol^{-1}. The HCOH and H_2CO species in their optimized positions as well as the water molecules involved in the proton transfer are highlighted in the ball and stick representation. The color code for the atoms is H in white, C in pale green, and O in red.

To get an estimate for this point, we have computed the crossover temperature (namely, the temperature below which tunneling dominates) adopting the formulation of Fermann & Auerbach (2000). Our estimation gives a crossover temperature of 194 K, and therefore this water-assisted proton transfer cannot be ruled out and might be feasible at the cryogenic temperature of the ISM via collective proton tunneling mechanisms (Drechsel-Grau & Marx 2014).

For the hydrogenation of $^2H_3C–C–OH_2$ (the product resulting from the reaction of CH_3 with the carbon reactive center), we found that only in Pos3 does the addition of H proceed in a barrierless way to form ethanol, whereas no spontaneous reactive events were observed in Pos1 and Pos2. This highlights the strong dependence of this kind of process on the different carbon binding sites (e.g., surface morphology, binding energies, or binding environments).

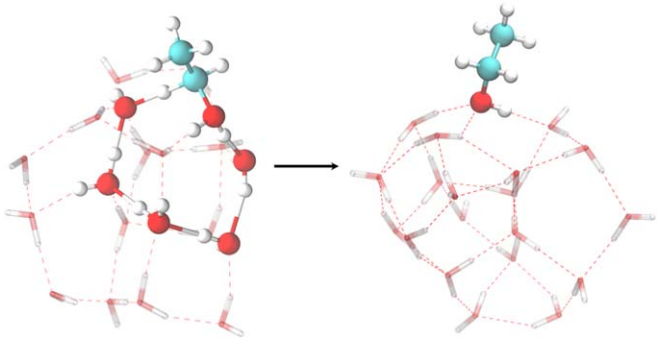

Figure 8. Snapshot of the geometric optimization representing the water-assisted proton transfer mechanism for the CH_3–H_2C–OH_2 → CH_3–CH_2–OH reaction and of the final product. The CH_3–CH_2–OH_2 species and the water molecules involved in the proton transfer are highlighted in the ball and stick representation (left structure) as well as ethanol in the optimized position (right structure). The color code for the atoms is H in white, C in pale green, and O in red.

The reaction forming ethanol can be written as

$$^2H_3CC–OH_2 + {}^2H \longrightarrow H_3CCH_2OH. \quad (11)$$

Like several cases shown in this work, the addition of H triggers a spontaneous water-assisted proton shuttle that allows the formation of ethanol as the final product, as shown in Figure 8.

NH_2. Finally, as far as the NH_2 radical is concerned, its addition to ^3C–OH_2 behaves differently than those for OH and CH_3. Indeed, the addition of NH_2 to Pos1 and Pos2 cleaves the original C–O bond during the optimization process and leads to the formation of the ^2C–NH_2 species (see Figure 9(A)). The reason is that, as in the O and N additions, the formed C–N bond presents an enhanced stability (reaction energy of -473 kJ mol^{-1}) with respect to the single C–O bond of the carbon reactive center, and accordingly, in the energy balance, the process is thermodynamically favorable. That is

$$^2NH_2 + {}^3C–OH_2 \longrightarrow {}^2NH_2\,C + H_2O. \quad (12)$$

From Pos3, however, the NH_2 radical adds to the carbon reactive center in a barrierless way and without breaking the original C–O bond, hence forming the ^2H_2N–COH_2 species (see Figure 9(B)). The reaction is thus

$$^2NH_2 + {}^3C–OH_2 \longrightarrow {}^2NH_2–C–OH_2. \quad (13)$$

For both species formed (namely, $^2NH_2C$ and $^2NH_2$–C–OH_2), we studied the addition of one H atom. Irrespective of the reactants, in both cases, the hydrogenation leads to the spontaneous formation of NH_2CH. On $^2NH_2C$, the H atom adds directly to the C atom, while on $^2NH_2$–C–OH_2, the addition of H to the C atom induces the cleavage of the C–O bond, releasing the initial icy H_2O molecule.

Interestingly, the NH_2CH species formed is the less stable isomer of methanimine (NH=CH_2), a molecule found in different interstellar environments (Godfrey et al. 1973; Dickens et al. 1997). Thus, we studied the isomerization reaction of NH_2CH → NH=CH_2 to check whether this transformation is feasible in the ISM. We ran an NEB calculation (only on Pos1) by considering a water-assisted proton transfer (results shown in Figure 10). As was found for the case of formaldehyde (see above), this process presents an energy barrier, in this case of 14 kJ mol^{-1} considering ZPE corrections. This energy barrier is insurmountable at cryogenic interstellar temperatures. However, as mentioned above, tunneling effects can make the reaction kinetically feasible. To check this point, we also computed here the crossover temperature, found to be 198 K. Thus, this route cannot be excluded, while a more rigorous kinetic treatment including nuclear quantum effects is necessary to have a definitive answer to this point.

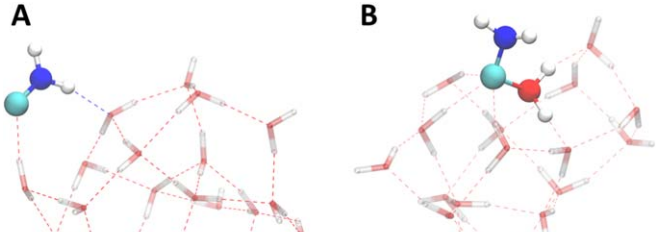

Figure 9. (A) ^2C–NH_2 species and (B) ^2H_2N–COH_2 species highlighted in the ball and stick representation in their optimized geometries. The color code for the atoms is H in white, C in pale green, N in blue, and O in red.

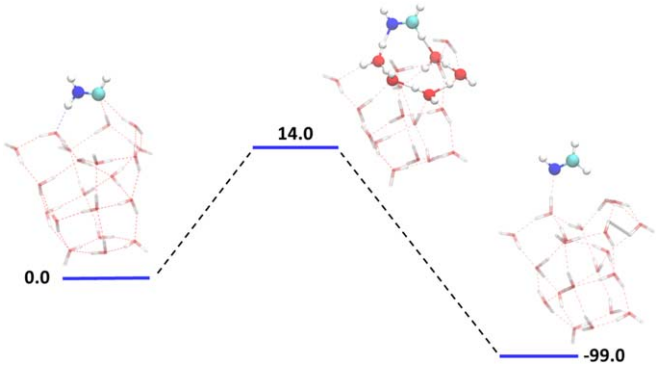

Figure 10. Energy diagram (i.e., reactant, TS, and product) representing the water-assisted proton transfer mechanism for the $HCNH_2$ → H_2CNH reaction. ZPE-corrected energies are reported in kJ mol^{-1}. The $HCNH_2$ and methanolimine (H_2CNH) species in their optimized positions, as well as the water molecules involved in the proton transfer, are highlighted in the ball and stick representation. The color code for the atoms is H in white, C in pale green, N in blue, and O in red.

4. Discussion and Astrophysical Implications

4.1. Carbon Reactivity and Reaction Products

According to the results above, the C (^3P) atom presents an extraordinary reactivity toward any H_2O molecule belonging to interstellar ice mantles, forming ^3C–OH_2 through the simple coupling of the C atom with the water molecule. This very first result has an important astrophysical implication: C atoms landing on water-dominated ice mantles do not remain as carbon atoms but are locked in the form of ^3C–OH_2, making difficult the occurrence of chemical reactions involving bare C atoms on water ice surfaces. However, this species keeps the triplet electronic spin state of the initial C atom, which is of fundamental importance for its chemical properties and reactivity. A summary of the chemical reactions presented in Section 3, alongside their energetic features (i.e., reaction energies and energy barriers if present), is reported in Table 2.

The ^3C–OH_2 carbon reactive center does not present any chemical reactivity when in proximity to the closed-shell species of CO, CO_2, NH_3, and H_2, implying that it remains as such once formed on the water ice mantles. However, in the presence of open-shell species such as atoms and molecular

Table 2
Summary of the Reactivity Investigated for the $^3C–OH_2$ Carbon Reactive Center with the Closed-shell Species NH_3, CO, CO_2, and H_2, the Atoms H, N, and O, and the Molecular Radicals OH, CH_3, and NH_2

Reactive Species	Reaction	$\Delta H_{rx}(0)$	$\Delta H^{\ddagger}(0)$
NH_3	No reaction	⋯	⋯
CO	No reaction	⋯	⋯
CO_2	No reaction	⋯	⋯
H_2	$H_2 + {}^3C–OH_2 \rightarrow {}^3CH_2 + H_2O$	−187.1	70.3
H	$H(^2S) + {}^3C–OH_2 \rightarrow {}^2HC–OH_2$	−358.6	Barrierless
	$^2HC–OH_2 \rightarrow {}^2CH + H_2O$	+149.5	⋯
Pos1	$H(^2S) + {}^2HC–OH_2 \rightarrow CH_3–OH$	−614.3	Barrierless
Pos2	$H(^2S) + {}^2HC–OH_2 \rightarrow CH_2–OH_2 \xrightarrow{NEB} CH_3–OH$	−601.7	Barrierless[a]
Pos3	$H(^2S) + {}^2HC–OH_2 \rightarrow CH_2–OH_2 \xrightarrow{NEB} CH_3–OH$	−638.8	Barrierless[a]
	$H(^2S) + {}^2HC–OH_2 \rightarrow {}^3CH_2 + H_2O$	−275.8	Barrierless
N	$N(^4S) + {}^3C–OH_2 \rightarrow {}^2CN + H_2O$	−683.9	Barrierless
O	$O(^3P) + {}^3C–OH_2 \rightarrow CO + H_2O$	−958.0	Barrierless
OH	$^2OH + {}^3C–OH_2 \rightarrow {}^2HO–C–OH_2$	−386.2	Barrierless
	$H(^2S) + {}^2HO–C–OH_2 \rightarrow HO–CH_2–OH$	−589.2	Barrierless
	$H(^2S) + {}^2HO–C–OH_2 \rightarrow HCOH + H_2O$	−388.8	Barrierless
	$HCOH \rightarrow H_2CO$	−170.1	7.6
CH_3	$^2CH_3 + {}^3C–OH_2 \rightarrow {}^2CH_3–C–OH_2$	−328.5	Barrierless
	$H(^2S) + {}^2CH_3–C–OH_2 \rightarrow CH_3CH_2OH$	−618.6	Barrierless
NH_2	$^2NH_2 + {}^3C–OH_2 \rightarrow {}^2C–NH_2 + H_2O$	−473.0	Barrierless
	$H(^2S) + {}^2C–NH_2 \rightarrow NH_2–CH$	−346.0	Barrierless
	$^2NH_2 + {}^3C–OH_2 \rightarrow {}^2NH_2–C–OH_2$	−475.5	Barrierless
	$H(^2S) + {}^2NH_2–C–OH_2 \rightarrow NH_2–CH + H_2O$	−270.1	Barrierless
	$NH_2–CH \rightarrow NH{=}CH_2$	−99.0	14.0

Notes. The subsequent reactions of the resulting products with H atoms are also shown. The superscripts indicate the electronic spin state of the species.
[a] The reaction presents a potential energy barrier $\leqslant 4$ kJ mol^{-1}, but when including ZPE corrections the barrier becomes submerged with respect to the reactants and, accordingly, it is barrierless.

radicals, it exhibits great chemical activity. As one can see in Table 2, most of the processes involving open-shell reactants are barrierless with very favorable reaction energies and, accordingly, are very feasible in the ISM conditions. This renders the $^3C–OH_2$ species a potential trigger for interstellar chemical diversity and complexity. However, it mostly leads to the formation of simple molecules, such as CO, CN, and CH_2, and only a few iCOMs are formed in this way: methanol, methanediol, and ethanol. Most of the studied reactions follow a chemical pattern toward the final formation of these compounds. That is, the $^3C–OH_2$ carbon reactive center reacts with the corresponding open-shell species and is followed by an addition of H, which results in the final product, usually involving a spontaneous (i.e., barrierless) water-assisted proton-transfer shuttle from the OH_2 moiety to the unsaturated atom. For instance, for the formation of CH_3CH_2OH, $^3C–OH_2$ reacts with $^2CH_3$ to form $^2CH_3–COH_2$, and a subsequent addition of H to the central C atom activates a spontaneous proton transfer assisted by water from the OH_2 group to the central C atom (see Figure 8). For those cases in which the water-assisted proton transfer is not spontaneous (i.e., presenting a barrier), which concern the formation of H_2CO and $NH{=}CH_2$ (see Table 2), the processes are expected to be kinetically feasible. Indeed, the barriers are not high (7.6 and 14.0 kJ mol^{-1}), and because of the involvement of the light H atom and the very low temperatures at which these reactions occur, tunneling effects should dominate the kinetics (as indicated by the crossover temperatures), thereby enabling the occurrence of these reactions.

It is worth mentioning, however, that all these results hold when the reactive species are in proximity. That is, for the barrierless processes, we observe spontaneous reactivity (e.g., direct chemical bond formation) when the two partners are separated by about 2.5 Å and the system is allowed to relax. If we consider that they take place adopting a Langmuir–Hinshelwood mechanism, the reactions are thus limited by the diffusivity of the reactants. This should not be a problem for the atomic species (H, O, and N) since they can diffuse on water ice surfaces at very low temperatures (e.g., Kuwahata et al. 2015; Senevirathne et al. 2017; Shimonishi et al. 2018; Pezzella & Meuwly 2019). However, this is not the case for the CH_3, NH_2, and OH radical species since, according to their binding energies (ranges of 9–13, 24–37, and 13–44 kJ mol^{-1}, respectively; Ferrero et al. 2020), they remain firmly attached to the surface with no chance to diffuse on the water ice surface at 10 K. Thus, the only way for these latter reactions to occur is that the carbon reactive center forms (i.e., the C atom lands on the ice surface) in the surroundings of these radicals, which can be present as icy species (previously formed by photolysis of relatively abundant icy components) or, alternatively, that the radicals form in the vicinity of an already formed $^3C–OH_2$ species.

In relation to this aspect of diffusion, it is also worth mentioning that the formation of $^3C–OH_2$ implies the

chemisorption of C atoms on water ice (Shimonishi et al. 2018; Molpeceres et al. 2021; Lamberts et al. 2022). This goes against the usual vision that C, as an atomic species, is physisorbed and, as such, presents some diffusivity on the surfaces. Our results indicate that this is not the case, because C is locked as ^{3}C–OH$_2$, which does not show mobility on the water ice surfaces, and should be considered in the future in the astrochemical models.

4.2. Comparison with Previous Studies

Formation of the ^{3}C–OH$_2$ species was also found in other works (Shimonishi et al. 2018; Molpeceres et al. 2021). A comparison with the work of Molpeceres et al. (2021) is needed to have a clear picture of the possible processes that can happen after the chemisorption of carbon on water ice mantles. In their work, a large set of C + H$_2$O(ice) reactions were studied because they sampled more initial positions. In 71% of the studied cases, they found, like in our work, the direct formation of the ^{3}C–OH$_2$ species, while in the remaining cases, they observed either the formation of the ^{3}[COH$^-$/H$_3$O$^+$] ion pair (19%) or the direct formation of ^{3}HCOH (10%), phenomena that are not observed in our (more limited) cases. Subsequently, they studied how the ^{3}C–OH$_2$ and the ion pair species can rearrange in ^{3}HCOH. They found out that both processes are feasible via a water-assisted proton transfer, the former presenting energy barriers that depend on the binding site, that is, very low or even barrierless in shallow C binding sites, or barriers of 9.7–11.5 kJ mol^{-1} in deeper C binding sites). The ion pair rearrangement was found to have a submerged barrier (e.g., barrierless) when including ZPE corrections. From the ^{3}HCOH species, they showed that formaldehyde (H$_2$CO) can be formed in a barrierless way but by passing through an ISC, involving a change in the spin state (from a triplet electronic state to the singlet one). Nevertheless, it is reasonable to think that the ^{3}C–OH$_2$, a relatively stable compound, can also react with the open-shell species in its proximity, forming the variety of compounds shown in this work, and these can be regarded as actual competitive processes to formaldehyde formation due to the restructuring of the ^{3}C–OH$_2$ carbon reactive center. The possible outcomes will depend strongly on the binding sites of the C atom and the surrounding structure of the ice.

4.3. Proton Transfer Process

An important aspect that allows the formation of the final products is the occurrence of water-assisted proton transfers. As highlighted in different works dealing with these processes (Rimola et al. 2018; Molpeceres et al. 2021; Perrero et al. 2022), this mechanism is efficient only if water molecules surrounding the carbon atom have a favorable orientation for the proton transfer, that is, the proton has to be transferred and the water molecules have to be connected by hydrogen bonds (H-bonds) that permit the proton shuttle by linking the initial position to the final one. In our reaction, this proper orientation is facilitated by the negative net charge of the C atom in the ^{2}H$_2$C–OH$_2$ species (as provided by the Löwdin atomic charges, see above), which converts the carbon atom into a good H-bond acceptor, which in this way forms part of the H-bond connectivity and receives the shuttled proton. It is worth mentioning that water-assisted mechanisms have been studied in other interstellar reactions, in which in some cases water molecules confer a strong catalytic effect (by reducing the energy barriers or even rendering them spontaneous, like in this work; Rimola et al. 2010, 2018; Molpeceres et al. 2021; Perrero et al. 2022), while in others the transfer exhibits high potential energy barriers (Enrique-Romero et al. 2019, 2020). The occurrence of one event or the other depends on the chemical nature of the H atom, that is, whether it has a proton-like or a radical-like character. If the former, the water-assisted mechanism is efficient, the transfer presenting low energy barriers, while if the latter, the process presents high energy barriers. In water-assisted processes involving proton-like atoms, the exchanged H atoms have positive net charges (and hence they are H$^+$ (proton)-like atoms) and accordingly, the transfer occurs through a set of breaking/making chemical bonds with more electronegative atoms (in our reactions, through the O atoms of the water molecules and the C atom with a negative net charge), in which transient H$_3$O$^+$ species are formed along the proton shuttle. These H$_3$O$^+$ are stabilized by the interaction with the surrounding water molecules, which makes the water-assisted proton transfer energetically favorable. In contrast, in water-assisted processes involving H radical-like atoms, during the H shuttle, the radical H$_3$O$^{\cdot}$ forms as a transient species, which is not stable (it tends to separate into H$_2$O + H$^{\cdot}$, see, e.g., Rimola et al. 2021); hence, in these cases, the water-assisted mechanism presents high energy barriers.

4.4. Dependence on the Local Structure of the Substrate

Another message that emerges from this work is the relevance of the local structure of the ice in the surroundings where the ^{3}C–OH$_2$ forms. In this work, three different positions have been considered (Pos1, Pos2, and Pos3); according to our results, Pos3 presents different environmental effects to Pos1 and Pos2. Obviously, robust statistics of the possible outcomes of the reactions cannot be reached with only the three studied cases. However, the molecular pictures provided here indicate that the icy water interactions with ^{3}C–OH$_2$ are important in modulating its chemical properties and reactivity. That is, the C atom of ^{3}C–OH$_2$ is engaged in three hydrogen bonds at Pos3, but in only two at Pos1 and Pos2 (see Figure 2 for comparison). Accordingly, ^{3}C–OH$_2$ at Pos3 presents an enhanced stabilization with respect to those at Pos1 and Pos2. Hence, it was found that the addition of the NH$_2$ radical to the ^{3}C–OH$_2$ at Pos1 and Pos2 results in the cleavage of the C–O bond (releasing the original H$_2$O molecule), while at Pos3 the ^{3}C–OH$_2$ species remains stable. Therefore, the structural environment around the carbon reactive center is an important aspect to take into consideration to understand its reactivity, since different routes can dominate according to the boundary conditions.

4.5. Methane Formation

Finally, this work also gives an atomistic interpretation of experiments performed in laboratories relative to the reactivity of atomic C in the presence of water ice surfaces. As mentioned in the Introduction, Qasim et al. (2020) found that methane (CH$_4$) was formed when C and H atoms and H$_2$O molecules were co-deposited at cryogenic temperatures. Although a priori our results go against these findings (because C on H$_2$O ice is locked in the form of ^{3}C–OH$_2$), this is not the case, and we provide the following mechanistic proposal toward CH$_4$ formation that reconciles theory and experiment. According to our results, a first addition of H to ^{3}C–OH$_2$ gives ^{2}HC–OH$_2$,

and a second addition of H forms CH_2–OH_2, which converts into CH_3OH through a spontaneous water-assisted proton transfer. This is true if the second addition of H is performed in a total singlet electronic state, i.e., the ^{2}HC–OH_2 and the H (^{2}S) present opposite electronic spins. However, if the reaction occurs in a total triplet electronic state (i.e., with the two partners presenting unpaired electrons having the same spin), the reaction gives $^3CH_2$–OH_2, which transforms spontaneously into $^3CH_2 + H_2O$, that is, it forms methylene ($^3CH_2$) and releases the original water. This process has been found to be barrierless and has a reaction energy of -245 kJ mol^{-1} (see Table 2), and thus it is feasible and competes with the singlet reaction. Accordingly, in the experiments, it is likely that atomic C condenses with H_2O, forming the ^{3}C–OH_2 carbon reactive center, the hydrogenation of which gives rise first to $^3CH_2$ and finally to CH_4. Unfortunately, experiments did not search for methanol so that we cannot say if it was found or not.

Our results are also in agreement with the work of Lamberts et al. (2022) on the reactivity of H_2 with C and CH_n species to form CH_4. We have computed the reaction $H_2 + {}^3$C–$OH_2 \rightarrow {}^3CH_2 + H_2O$ in our cluster model and it presents an energy barrier of 70 kJ mol^{-1}. This value is very close to the value found in Lamberts et al. (2022) for the reaction in the presence of an $(H_2O)_3$ minimal cluster model. These values of energy barrier are extremely high to occur in the ISM, even if tunneling could dominate. Thus, this path to form CH_4 can be excluded as concluded in Lamberts et al. (2022). A likely possibility already pointed out in the work of Lamberts et al. (2022) is that the ^{2}CH–OH_2 species is formed first, and reaction with H_2 gives rise to CH_3 and H_2O, the former species giving rise to CH_4 upon hydrogenation.

4.6. Astrophysical Implications

Since the pioneering work by Garrod & Herbst (2006), astrochemical models have preferred the scheme of radical–radical combination and/or hydrogenation of molecules on grain-surfaces for the synthesis of iCOMs. The former reaction scheme postulates that radicals diffuse over the grain-surfaces upon the increase in temperature of the dust grains caused by the birth of a protostar. However, this scheme has been challenged by the detection of iCOMs in protostellar shocks (e.g., Arce et al. 2008; Codella et al. 2009, 2017; Lefloch et al. 2017; De Simone et al. 2020) and cold objects (e.g., Bacmann et al. 2012; Cernicharo et al. 2012; Vastel et al. 2014; Scibelli & Shirley 2020), where the dust temperature has never increased and, consequently, radicals could not migrate. Additionally, QM calculations show that the radical–radical combination does not necessarily lead to the formation of iCOMs (Enrique-Romero et al. 2021, 2022).

Alternative possibilities have been proposed, such as nondiffusive processes occurring on the grain-surfaces (Jin & Garrod 2020; Garrod et al. 2022) and the formation of iCOMs in the gas phase (Vasyunin & Herbst 2013; Balucani et al. 2015; Skouteris et al. 2017, 2018).

Another possibility is the one studied in this work, namely that gaseous species landing react instantaneously with the frozen molecules of the grain mantles. Given their abundances, water and CO are the two major possible ice molecules. Previous works have shown that this is a viable path to synthesize formamide and ethanol on H_2O-rich ice (Rimola et al. 2018; Perrero et al. 2022) and acetaldehyde and ethanol on CO-rich ice (Ferrero et al. 2023a). In this work, we have examined the possible formation of iCOMs from gaseous C atoms landing on H_2O-rich ices, which gives rise to the formation of the very reactive, and nondiffusive, species ^{3}C–OH_2 (see also Shimonishi et al. 2018; Molpeceres et al. 2021). In turn, this species could react with landing or nearby atoms and molecules. Here we considered the most abundant of them and found that some reactions lead to small species while only methanol, methanediol, and ethanol can be formed in this way.

Therefore, another process beyond CO hydrogenation can produce methanol on the grain-surfaces, started by C atoms landing on H_2O-rich ice. This is a potentially important contribution to the formation of methanol in regions where C and not CO is abundant, notably the photodissociation regions (PDRs) and in the early stages of the chemical evolution of molecular clouds from diffuse atomic ones. Gaseous methanol has indeed been observed in these regions (see, e.g., the discussion in Bouvier et al. 2020). We have to emphasize that, assuming that the process found here to form frozen methanol is the dominant one in CO-poor/C-rich regions, some nonthermal mechanism must be at work to inject it into the gas phase. In this sense, three mechanisms are evoked in the literature: photodesorption, reactive desorption, and cosmic-ray-induced desorption. However, all of them seem to have drawbacks. UV-induced photodesorption does break the methanol into small pieces (Bertin et al. 2016), reactive desorption does not seem to be efficient (Pantaleone et al. 2020), and neither does cosmic-ray-induced desorption (Wakelam et al. 2021).

Methanediol has not yet been detected in the ISM (McGuire 2022), perhaps because the frequencies of its rotational transitions are not available in the two astronomical databases at CDMS[5] (Endres et al. 2016) and JPL[6] (Pickett et al. 1998). Probably, its detection (even with JWST) in the solid phase is unlikely because of the a priori low abundance and also because the frequencies are likely in a heavily crowded region of the spectrum. It will be worth searching for this molecule in the gas phase: if a nonthermal mechanism injects methanol, then it is likely that also some methanediol will be gaseous.

Finally, our work shows that ethanol can be synthesized on the H_2O-rich ice grain-surfaces in CO-poor/C-rich regions, i.e., in PDRs and in the early stages of the chemical evolution of molecular clouds from diffuse atomic ones. Perrero et al. (2022) have already shown that ethanol can be formed on the grain-surfaces in H_2O-rich ices by the reaction of CCH with an icy water molecule, followed by hydrogenation. In addition, Enrique-Romero et al. (2022) have shown that the coupling of CH_3 and CH_2OH on the grain-surfaces may also lead to ethanol. Thus, there are at least three different grain-surface paths that lead to the formation of ethanol. In the astrochemical gas-phase reaction networks, ethanol can be formed either by the electron recombination of protonated ethanol or the reaction of acetone with H_3^+.[7] Considering the gaseous abundances of C, CCH, protonated ethanol, and acetone and the likely frozen abundances of CH_3 and CH_2OH, the most efficient way to form ethanol is likely on the grain-surfaces via the reactions involving C and CCH, whose abundances can reach a

[5] https://cdms.astro.uni-koeln.de/cgi-bin/cdmssearch
[6] https://spec.jpl.nasa.gov/ftp/pub/catalog/catform.html
[7] http://udfa.ajmarkwick.net/

maximum of about 10^{-4} and 10^{-8} (with respect to H nuclei), respectively. Moreover, it is possible that the path involving carbon atoms, studied here, is the dominant way to form ethanol. Remarkably, ethanol is the only iCOM in addition to methanol that may have been detected in the solid form (Yang et al. 2022; McClure et al. 2023). Also remarkably, ethanol is supposed to be the mother of some iconic iCOMs—glycolaldehyde and acetaldehyde (Skouteris et al. 2018; Vazart et al. 2020)—once injected into the gas phase.

5. Conclusions

In this work, the reactivity of atomic C on water ice has been studied by means of quantum chemical computations. It is shown that the C atom in its ground state (^{3}P) is reactive upon water ice adsorption, forming the ^{3}C–OH$_2$ species, which remains anchored to the water ice. Then, possible subsequent reactions with closed-shell species (i.e., CO, CO_2, NH_3, and H_2), atoms (i.e., H(^{1}S), N(^{4}S), and O(^{3}P)) and radicals (i.e., OH, NH_2, and CH_3) have been considered.

It has been found that ^{3}C–OH$_2$ does not present reactivity with the closed-shell species, but it is highly reactive with the atoms and molecular radicals. Some reactions form small molecules, such as CN and CO. Others lead to the formation of three iCOMs spontaneously, in a barrierless process: methanol (CH_3OH), methanediol ($HOCH_2OH$), and ethanol (CH_3CH_2OH). In addition, the formation of H_2CO and $NH{=}CH_2$ exhibits energy barriers not surmountable at cryogenic temperatures, but they might be formed via tunneling, as indicated by the respective calculated crossover temperatures. In view of the low energy requirements of these chemical reactions, the processes are limited by diffusion, which for the molecular radicals is an important issue due to their low diffusivity. Accordingly, the reactions are feasible if the two partners are in proximity in cold environments.

In the formation of most of these species, water ice actively participates in the reaction thanks to water-assisted proton transfers. They happen in a barrierless way at low ISM temperatures but only work if the icy water components present a suitable hydrogen bond connection that allows the proton exchange.

The work also shows the role of icy grains as concentrators of C in an activated form, since the ^{3}C–OH$_2$ species is highly reactive with open-shell species. To the best of our knowledge, this feature is not particularly developed in astrochemical models because atomic C is usually considered to be physisorbed on ice surfaces. This also affects the diffusion properties of C, since it is completely hindered, at variance to what would occur if it were physisorbed.

From the astrochemical context, according to our results, it seems that CH_4 cannot form by multiple hydrogenations of atomic C on water ice mantles because it is locked in the form of ^{3}C–OH$_2$. However, the great reactivity of this species allows a likely final formation of CH_4 (as observed in the experiments of Qasim et al. 2020). This is achieved once the ^{3}C–OH$_2$ species is formed, as its subsequent hydrogenation (i.e., reaction with H (^{2}S)) gives rise to first the ^{2}CH–OH$_2$ intermediate and then ^{3}CH$_2$–OH$_2$ (if the reaction takes place in a triplet total electronic spin state), which decomposes spontaneously into $^3CH_2 + H_2O$. Two additions of H on the generated $^3CH_2$ result in the formation of CH_4. Our results also agree with the work of Lamberts et al. (2022), which rules out the reactivity of molecular hydrogen (H_2) with C as a reactive channel toward CH_4 formation. In our case, the reaction of H_2 with the ^{3}C–OH$_2$ to give $^3CH_2 + H_2O$ presents a huge energy barrier insurmountable in ISM conditions.

Finally, this work is particularly relevant for the formation of methanol and ethanol in CO-poor/C-rich regions, such as PDRs or in the early chemical evolution of molecular clouds. When taking into account the different proposed routes to form ethanol and the abundances of the reactants, we showed that the one involving atomic carbon and water ice molecules, as studied here, could be the dominant one.

Acknowledgments

This project has received funding from the Marie Sklodowska-Curie Action (MSCA) for the project "Astro-Chemical Origins" (ACO), grant agreement No. 811312, and within the European Union's Horizon 2020 research and innovation program from the European Research Council (ERC) for the projects "The Dawn of Organic Chemistry" (DOC), grant agreement No. 741002, and "Quantum Chemistry on Interstellar Grains" (QUANTUM-GRAIN), grant agreement No. 865657. MICIN (project PID2021-126427NB-I00) is also acknowledged. The Italian Space Agency for co-funding the Life in Space Project (ASI N. 2019-3-U.O) and the Italian MUR (PRIN 2020, Astrochemistry beyond the second period elements, Prot. 2020AFB3FX) are also acknowledged for financial support. The authors acknowledge support from the Project CH4.0 under the MUR program "Dipartimenti di Eccellenza 2023-2027" (CUP: D13C22003520001). We also thankfully acknowledge the computer resources and assistance provided by the Barcelona Supercomputing Center (BSC) and CSUC.

ORCID iDs

Stefano Ferrero https://orcid.org/0000-0001-7819-7657
Cecilia Ceccarelli https://orcid.org/0000-0001-9664-6292
Piero Ugliengo https://orcid.org/0000-0001-8886-9832
Mariona Sodupe https://orcid.org/0000-0003-0276-0524
Albert Rimola https://orcid.org/0000-0002-9637-4554

References

Allen, M., & Robinson, G. W. 1975, ApJ, 195, 81
Andersson, S., Goumans, T. P. M., & Arnaldsson, A. 2011, CPL, 513, 31
Arce, H. G., Santiago-García, J., Jørgensen, J. K., Tafalla, M., & Bachiller, R. 2008, ApJL, 681, L21
Ásgeirsson, V., Birgisson, B. O., Bjornsson, R., et al. 2021, J. Chem. Theory Comput., 17, 4929
Bacmann, A., Taquet, V., Faure, A., Kahane, C., & Ceccarelli, C. 2012, A&A, 541, L12
Balucani, N., Ceccarelli, C., & Taquet, V. 2015, MNRAS, 449, L16
Bernstein, M. P., Sandford, S. A., Allamandola, L. J., Chang, S., & Scharberg, M. A. 1995, ApJ, 454, 327
Bernstein, M. P., Sandford, S. A., Allamandola, L. J., et al. 1999, Sci, 283, 1135
Bertin, M., Romanzin, C., Doronin, M., et al. 2016, ApJL, 817, L12
Blake, G. A., Sutton, E. C., Masson, C. R., & Phillips, T. G. 1987, ApJ, 315, 621
Boogert, A. A., Gerakines, P. A., & Whittet, D. C. 2015, ARA&A, 53, 541
Bouvier, M., López-Sepulcre, A., Ceccarelli, C., et al. 2020, A&A, 636, A19
Cazaux, S., Tielens, A. G. G. M., Ceccarelli, C., et al. 2003, ApJL, 593, L51
Ceccarelli, C., Caselli, P., Fontani, F., et al. 2017, ApJ, 850, 176
Ceccarelli, C., Codella, C., Balucani, N., et al. 2023, in ASP Conf. Ser. 534, Protostars and Planets VII, ed. S. Inutsuka et al. (San Francisco, CA: ASP), 379
Ceccarelli, C., Loinard, L., Castets, A., Faure, A., & Lefloch, B. 2000, A&A, 362, 1122
Cernicharo, J., Marcelino, N., Roueff, E., et al. 2012, ApJL, 759, L43
Codella, C., Benedettini, M., Beltrán, M. T., et al. 2009, A&A, 507, L25
Codella, C., Ceccarelli, C., Caselli, P., et al. 2017, A&A, 605, L3

Cuppen, H. M., Walsh, C., Lamberts, T., et al. 2017, SSRv, 212, 1
De Simone, M., Codella, C., Ceccarelli, C., et al. 2020, A&A, 640, A75
Dickens, J. E., Irvine, W. M., DeVries, C. H., & Ohishi, M. 1997, ApJ, 479, 307
Drechsel-Grau, C., & Marx, D. 2014, PhRvL, 112, 148302
Duley, W. W., Millar, T. J., & Williams, D. A. 1978, MNRAS, 185, 915
Endres, C. P., Schlemmer, S., Schilke, P., Stutzki, J., & Müller, H. S. P. 2016, JMoSp, 327, 95
Enrique-Romero, J., Álvarez Barcia, S., Kolb, F. J., et al. 2020, MNRAS, 493, 2523
Enrique-Romero, J., Ceccarelli, C., Rimola, A., et al. 2021, A&A, 655, A9
Enrique-Romero, J., Rimola, A., Ceccarelli, C., et al. 2019, ESC, 3, 2158
Enrique-Romero, J., Rimola, A., Ceccarelli, C., et al. 2022, ApJS, 259, 39
Favre, C., Fedele, D., Semenov, D., et al. 2018, ApJL, 862, L2
Fedoseev, G., Qasim, D., Chuang, K.-J., et al. 2022, ApJ, 924, 110
Fermann, J. T., & Auerbach, S. 2000, JChPh, 112, 6787
Ferrero, S., Ceccarelli, C., Ugliengo, P., Sodupe, M., & Rimola, A. 2023a, ApJ, 951, 150
Ferrero, S., Pantaleone, S., Ceccarelli, C., et al. 2023b, ApJ, 944, 142
Ferrero, S., Zamirri, L., Ceccarelli, C., et al. 2020, ApJ, 904, 11
Garrod, R. T. 2013, ApJ, 765, 60
Garrod, R. T., & Herbst, E. 2006, A&A, 457, 927
Garrod, R. T., Jin, M., Matis, K. A., et al. 2022, ApJS, 259, 1
Godfrey, P. D., Brown, R. D., Robinson, B. J., & Sinclair, M. W. 1973, ApL, 13, 119
Goerigk, L., Hansen, A., Bauer, C., et al. 2017, PCCP, 19, 32184
Hama, T., & Watanabe, N. 2013, ChRv, 113, 8783
Henkel, C., Jacq, T., Mauersberger, R., Menten, K. M., & Steppe, H. 1987, A&A, 188, L1
Henning, T. 2010, ARA&A, 48, 21
Henning, T. K., & Krasnokutski, S. A. 2019, NatAs, 3, 568
Herbst, E., & van Dishoeck, E. F. 2009, ARA&A, 47, 427
Humphrey, W., Dalke, A., & Schulten, K. 1996, J. Mol. Graph., 14, 33
Hwang, D.-Y., Mebel, A. M., & Wang, B.-C. 1999, ChPhy, 244, 143
Ilee, J. D., Walsh, C., Booth, A. S., et al. 2021, ApJS, 257, 9
Iqbal, W., & Wakelam, V. 2018, A&A, 615, A20
Jin, M., & Garrod, R. T. 2020, ApJS, 249, 26
Jones, A. P., Fanciullo, L., Köhler, M., et al. 2013, A&A, 558, A62
Jones, A. P., Köhler, M., Ysard, N., Bocchio, M., & Verstraete, L. 2017, A&A, 602, A46
Jørgensen, J. K., Belloche, A., & Garrod, R. T. 2020, ARA&A, 58, 727
Krasnokutski, S. A., Chuang, K.-J., Jäger, C., Ueberschaar, N., & Henning, T. 2022, NatAs, 6, 381
Krasnokutski, S. A., Goulart, M., Gordon, E. B., et al. 2017, ApJ, 847, 89
Krasnokutski, S. A., Jäger, C., & Henning, T. 2020, ApJ, 889, 67
Kruse, H., & Grimme, S. 2012, JChPh, 136, 154101
Kuwahata, K., Hama, T., Kouchi, A., & Watanabe, N. 2015, PhRvL, 115, 133201
Lamberts, T., Fedoseev, G., van Hemert, M. C., et al. 2022, ApJ, 928, 48
Lefloch, B., Ceccarelli, C., Codella, C., et al. 2017, MNRAS, 469, L73
Liu, B., & McLean, A. D. 1973, JChPh, 59, 4557
Martín, S., Mangum, J. G., Harada, N., et al. 2021, A&A, 656, A46
McClure, M. K., Rocha, W. R. M., Pontoppidan, K. M., et al. 2023, NatAs, 7, 431
McGuire, B. A. 2022, ApJS, 259, 30
Meisner, J., & Kästner, J. 2016, Angew. Chem. Int. Ed., 55, 5400
Meisner, J., Lamberts, T., & Kästner, J. 2017, ESC, 1, 399
Miksch, A. M., Riffelt, A., Oliveira, R., Kästner, J., & Molpeceres, G. 2021, MNRAS, 505, 3157
Molpeceres, G., Jiménez-Serra, I., Oba, Y., et al. 2022, A&A, 663, A41
Molpeceres, G., & Kästner, J. 2021, ApJ, 910, 55
Molpeceres, G., Kästner, J., Fedoseev, G., et al. 2021, J. Phys. Chem. Lett., 12, 10854
Molpeceres, G., & Rivilla, V. M. 2022, A&A, 665, A27
Molpeceres, G., Rivilla, V. M., Furuya, K., et al. 2023a, MNRAS, 521, 6061
Molpeceres, G., Zaverkin, V., Furuya, K., Aikawa, Y., & Kästner, J. 2023b, A&A, 673, A51
Muller, S., Beelen, A., Guélin, M., et al. 2011, A&A, 535, A103
Neese, F., Wennmohs, F., Becker, U., & Riplinger, C. 2020, JChPh, 152, 224108
Öberg, K. I. 2016, ChRv, 116, 9631
Öberg, K. I., Guzmán, V. V., Furuya, K., et al. 2015, Natur, 520, 198
Palumbo, M. E., Castorina, A. C., & Strazzulla, G. 1999, A&A, 342, 551
Pantaleone, S., Enrique-Romero, J., Ceccarelli, C., et al. 2020, ApJ, 897, 56
Pantaleone, S., Enrique-Romero, J., Ceccarelli, C., et al. 2021, ApJ, 917, 49
Perrero, J., Enrique-Romero, J., Martínez-Bachs, B., et al. 2022, ESC, 6, 496
Pezzella, M., & Meuwly, M. 2019, PCCP, 21, 6247
Pickett, H. M., Poynter, R. L., Cohen, E. A., et al. 1998, JQSRT, 60, 883
Potapov, A., Krasnokutski, S. A., Jäger, C., & Henning, T. 2021, ApJ, 920, 111
Qasim, D., Fedoseev, G., Chuang, K. J., et al. 2020, NatAs, 4, 781
Rimola, A., Ceccarelli, C., Balucani, N., & Ugliengo, P. 2021, FrASS, 8, 655405
Rimola, A., Skouteris, D., Balucani, N., et al. 2018, ESC, 2, 720
Rimola, A., Sodupe, M., & Ugliengo, P. 2010, PCCP, 12, 5285
Rubin, R. H., Swenson, G. W., Jr., Benson, R. C., Tigelaar, H. L., & Flygare, W. H. 1971, ApJL, 169, L39
Schutte, W. A., Allamandola, L. J., & Sandford, S. A. 1992, AdSpR, 12, 47
Scibelli, S., & Shirley, Y. 2020, ApJ, 891, 73
Senevirathne, B., Andersson, S., Dulieu, F., & Nyman, G. 2017, MolAs, 6, 59
Shimonishi, T., Nakatani, N., Furuya, K., & Hama, T. 2018, ApJ, 855, 27
Skouteris, D., Balucani, N., Ceccarelli, C., et al. 2018, ApJ, 854, 135
Skouteris, D., Vazart, F., Ceccarelli, C., et al. 2017, MNRAS, 468, L1
Strazzulla, G. 1997, AdSpR, 19, 1077
Suzuki, T., Majumdar, L., Ohishi, M., et al. 2018, ApJ, 863, 51
Taquet, V., Ceccarelli, C., & Kahane, C. 2012, A&A, 538, A42
Tielens, A. G. G. M., & Hagen, W. 1982, A&A, 114, 245
Tsuge, M., Molpeceres, G., Aikawa, Y., & Watanabe, N. 2023, NatAs, 847, 89
Vastel, C., Ceccarelli, C., Lefloch, B., & Bachiller, R. 2014, ApJL, 795, L2
Vasyunin, A. I., & Herbst, E. 2013, ApJ, 769, 34
Vazart, F., Ceccarelli, C., Balucani, N., Bianchi, E., & Skouteris, D. 2020, MNRAS, 499, 5547
Vydrov, O. A., & Van Voorhis, T. 2010, JChPh, 133, 244103
Wakelam, V., Dartois, E., Chabot, M., et al. 2021, A&A, 652, A63
Walsh, C., Loomis, R. A., Öberg, K. I., et al. 2016, ApJL, 823, L10
Watanabe, N., & Kouchi, A. 2008, PrSS, 83, 439
Weigend, F., & Ahlrichs, R. 2005, PCCP, 7, 3297
Woon, D. E. 2021, AcChR, 54, 490
Yang, Y.-L., Green, J. D., Pontoppidan, K. M., et al. 2022, ApJL, 941, L13
Zamirri, L., Ugliengo, P., Ceccarelli, C., & Rimola, A. 2019, ESC, 3, 1499